ELSEVIER

Contents lists available at ScienceDirect

Carbohydrate Polymers

journal homepage: www.elsevier.com/locate/carbpol





Nanopore-regulated *in situ* polymerization for synthesis of homogeneous heparan sulfate with low dispersity

Meng Qiao ^{a,1}, Zhe Wang ^{b,1}, Junjie Zhang ^a, Yanqi Li ^a, Liang-An Chen ^c, Fuming Zhang ^d, Jonathan S. Dordick ^d, Robert J. Linhardt ^{d,e}, Chao Cai ^{b,*}, He Huang ^a, Xing Zhang ^{a,*}

- ^a School of Food Science and Pharmaceutical Engineering, Nanjing Normal University, Nanjing 210023, China
- b Key Laboratory of Marine Drugs of Ministry of Education, Shandong Provincial Key Laboratory of Glycoscience and Glycotechnology, School of Medicine and Pharmacy, Ocean University of China, Qingdao 266003, China
- ^c Jiangsu Collaborative Innovation Center of Biomedical Functional Materials, Jiangsu Key Laboratory of New Power Batteries, School of Chemistry and Materials Science, Nanjing Normal University, Nanjing 210023, China
- d Departments of Chemical and Biological Engineering, and Biological Sciences, Center for Biotechnology and Interdisciplinary Studies, Rensselaer Polytechnic Institute, Troy, NY 12180, USA
- ^e Department of Chemistry and Chemical Biology, Rensselaer Polytechnic Institute, Troy, NY 12180, USA

ARTICLE INFO

Keywords: Homogeneous heparan sulfate Metal-organic capsule Enzyme immobilization Glycosylation reaction

ABSTRACT

The biological activities of heparan sulfate (HS) are intimately related to their molecular weights, degree and pattern of sulfation and homogeneity. The existing methods for synthesizing homogeneous sugar chains of low dispersity involve multiple steps and require stepwise isolation and purification processes. Here, we designed a mesoporous metal-organic capsule for the encapsulation of glycosyltransferase and obtained a microreactor capable of enzymatically catalyzing polymerization reactions to prepare homogeneous heparosan of low dispersity, the precursor of HS and heparin. Since the sugar chain extension occurs in the pores of the microreactor, low molecular weight heparosan can be synthesized through space-restricted catalysis. Moreover, the glycosylation co-product, uridine diphosphate (UDP), can be chelated with the exposed metal sites of the metalorganic capsule, which inhibits trans-cleavage to reduce the molecular weight dispersity. This microreactor offers the advantages of efficiency, reusability, and obviates the need for stepwise isolation and purification processes. Using the synthesized heparosan, we further successfully prepared homogeneous 6-O-sulfated HS of low dispersity with a molecular weight of approximately 6 kDa and a polydispersity index (PDI) of 1.032. Notably, the HS generated exhibited minimal anticoagulant activity, and its binding affinity to fibroblast growth factor 1 was comparable to that of low molecular weight heparins.

1. Introduction

Heparan sulfate (HS)/heparin is a class of sophisticated, polydisperse acidic polysaccharides composed of alternating residues of hexosamine (HexN) and uronic acid (UA). HexN residues encompass glucosamine (GlcN), *N*-acetylglucosamine (GlcNAc), or their sulfated derivatives, such as *O*-sulfo-HexN or *N*-sulfoglucosamine (GlcNS), while UA includes glucuronic acid (GlcA), iduronic acid (IdoA), and its 2-*O*-sulfo derivatives (GlcA2S and IdoA2S) (Fig. 1A) (Mende et al., 2016; Zhang et al., 2020). Heparin is a highly sulfated form of HS. As an essential glycosaminoglycan (GAG), HS/heparin possesses a variety of pharmacological activities, including anticoagulant, anti-inflammation, and

anticancer (Arnold et al., 2020; Clausen et al., 2020; Wang et al., 2022; Zhang et al., 2018). However, the functionality of HS/heparin is significantly influenced by its molecular features such as molecular weight and heterogeneity of sulfation. Meanwhile, as naturally sourced heparin typically possesses very poor uniformity, variations in the active ingredients across different batches may occur, leading to inaccurate medication dosages and posing safety risks (McGowan et al., 2016). Low molecular weight heparin (LMWH) has significant advantages in preventing venous thrombosis due to its longer half-life and more predictable anticoagulant dosing (Xu et al., 2011; Xu et al., 2014). Therefore, the development of structurally defined low molecular weight (LMW) HS/heparin is highly necessary to facilitate the investigation of HS-

^{*} Corresponding authors.

E-mail addresses: caic@ouc.edu.cn (C. Cai), zhangxing@njnu.edu.cn (X. Zhang).

¹ M.Q. and Z.W. contributed equally.

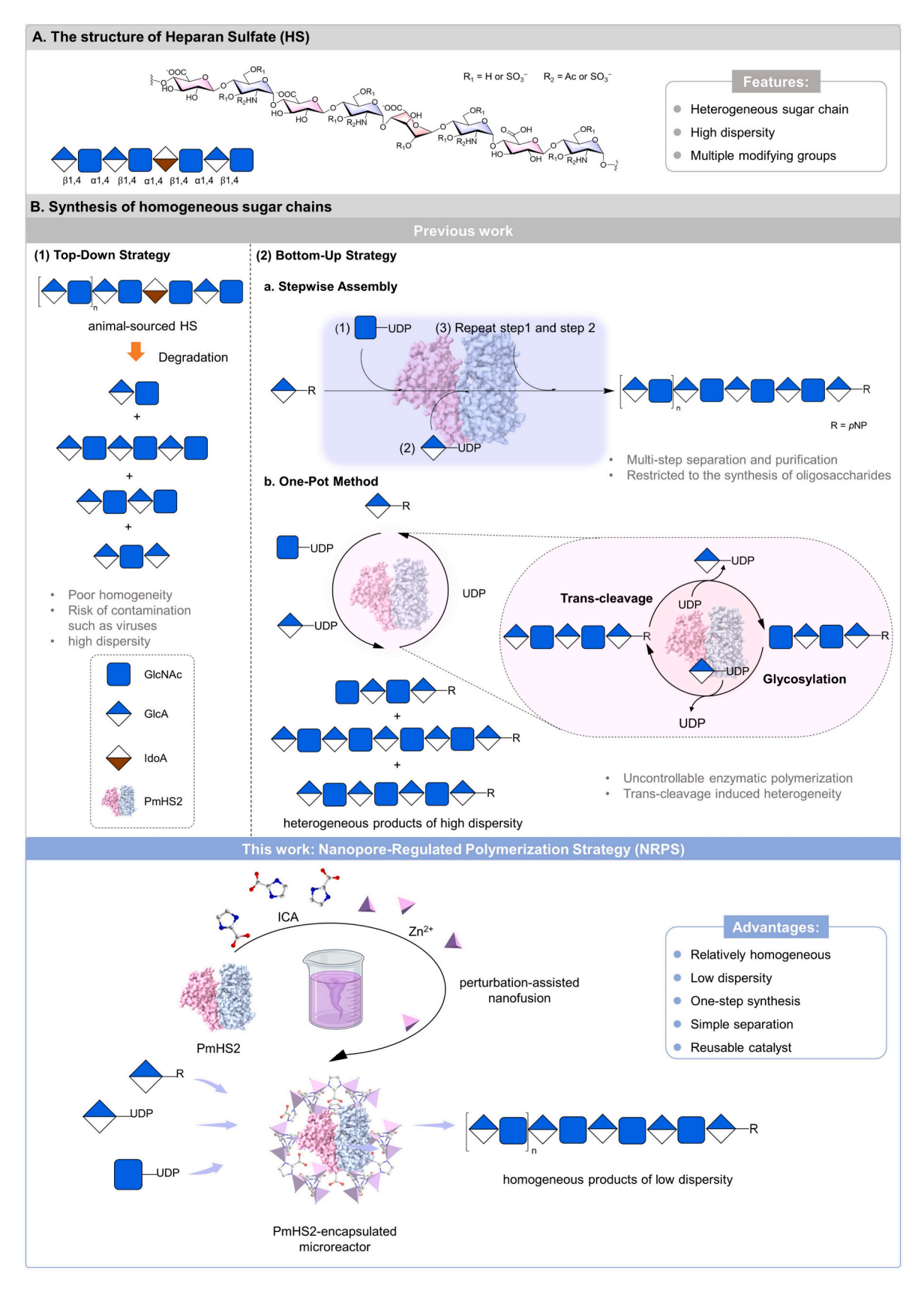


Fig. 1. The background and development of the preparation of HS. (A) The structure and features of HS. (B) Comparison of the synthesis methods of homogeneous sugar chains of low dispersity. The non-reducing ends is either GlcA or GlcNAc residues since PmHS2 is a bifunctional enzyme.

related biological activities and clinical application (Pawar et al., 2019; Wang et al., 2021).

Currently, the commercial preparation of LMWH relies on a top-down strategy involving the chemical or enzymatic degradation of heparin extracted from animal tissues (Fig. 1B1). This method has limitations such as highly disperse molecular weight, poor degradation controllability, intricate separation procedures, and potential risks of contamination with other glycosaminoglycans (GAGs), bacteria, or viruses (Liu et al., 2009). Therefore, the preparation of LMWH/LMW-HS through a bottom-up strategy, including the solid-phase method, is more promising to obtain homogeneous polysaccharides of low dispersity (Stancanelli et al., 2024). Although stepwise chemical or enzymatic assembly can prepare a structurally accurate sugar chain, both approaches are constrained by repetitive synthetic steps, intricate purification procedures, and low yields, and are unsuitable for the preparation of oligosaccharides larger than pentasaccharides (Fig. 1B2a) (Spadarella et al., 2020).

A one-pot enzymatic *co*-polymerization employing bifunctional gly-cosyltransferases presents the advantage of bypassing intermediate isolation and purification steps (Fig. 1B2b) (Li et al., 2017; Wang et al., 2020). However, the molecular weight distribution of the biocatalytic products is usually unsatisfactory, primarily due to: i) the uncontrollable enzymatic polymerization reaction that leads to over-elongation of sugar chains; ii) and the glycosylation co-product uridine diphosphate (UDP) that can inhibit the forward progression of the reaction and induce random trans-cleavage of the glycosidic bond of the sugar chain, amplifying polysaccharide dispersity. For instance, our previous study demonstrated that enzymatic polymerization with a nonasaccharide as acceptor results the desired decasaccharide but also some shorter saccharides (Zhang et al., 2017).

Metal-organic frameworks (MOFs) are porous crystalline materials constructed by the coordination of organic ligands with metal ions or clusters, and have been widely used for enzyme encapsulation and biocatalysis (An et al., 2020; Arbulu et al., 2018; Chen et al., 2018; Huang, Kou, Shen, Chen, Ouyang, 2020a, 2020b; Liu et al., 2020). In previous work, we successfully immobilized a series of glycosyltransferases, leading to an enhancement in both catalytic stability and activity (Qiao et al., 2022). The "armor-like" porous MOF exoskeleton tightly protects enzymes against an often deleterious external environment (Chen et al., 2020; Huang, Kou, Shen, Chen, Ouyang, 2020a, 2020b). Interestingly, as the enzymatic polymerization occurs within the space-constrained MOF, this armor has the potential to restrict the polymerization of sugar chains to obtain relatively low molecular weight polysaccharides. Meanwhile, MOFs with exposed metal sites can chelate the negatively charged UDP, thereby inhibiting undesired transcleavage.

Here, we employ a <u>n</u>anopore-<u>regulated</u> <u>polymerization strategy</u> (NRPS) to fabricate the synthesis of homogeneous sugar chains of low dispersity. We devise a mesoporous metal-organic capsule using perturbation-assisted nanofusion to encapsulate *Pasteurella multocida* heparosan synthase 2 (PmHS2), which is an essential dual-function glycosyltransferase in the enzymatic synthesis of HS (Yue et al., 2013; Yue et al., 2015). The microreactor was then employed to catalyze polymerization to heparosan. Critically, the UDP co-product was chelated by the MOF, thus reducing undesirable trans-cleavage. Ultimately, a homogeneous 6-O-sulfated LMW-HS of low dispersity was rapidly assembled based on this NRPS and showed comparable affinity to commercial LMWH drug enoxaparin for fibroblast growth factors (FGFs).

2. Results and discussion

The application of MOF-based *in situ* encapsulation of glycosyltransferases is limited by poor enzyme stability, requirement of a water-soluble ligand, and use of mild synthesis conditions at low temperatures. Based on our experience in immobilizing glycosyltransferases, Zn²⁺ and

2-imidazolecarboxaldehyde (ICA) were selected as the metal ion and organic ligand, which are compatible with glycosyltransferases. Meanwhile, the perturbation-assisted nanofusion method was used to prepare mesopore enzyme-encapsulated microreactors. The procedure involved vigorous stirring of a mixture aqueous solution of organic linker, enzyme, and metal ion precursor, resulting in the formation of mesoporous aggregates comprising nanosized MOFs. Modulation of the ratio of metal ion to organic ligand resulted in a finely tuned pore size in MOF. The PmHS2-encapsulated MOF materials with a metal-to-ligand ratio of 1:1 were designated as microreactor 1N, while those with a ratio of 1:2 were labeled as microreactor 2N, and so forth, extending to microreactor 3N, 4N, and 5N. The crystallinity of the synthesized PmHS2encapsulated microreactors was determined by powder X-ray diffraction (PXRD). The PXRD pattern of microreactors shows that the positions and intensities of all peaks shifted, indicating that a new phase and amorphous components are obtained after vigorous stirring and the enzyme involved while maintaining the crystallinity (Fig. 2A). The mesostructure of representative microreactor 4N was demonstrated by scanning electron microscopy (SEM), revealing the formation of uniformly shaped microspheres (Fig. 2D-E). Specifically, microreactor 4N exhibits a rough surface and an abundant pore structure, which is conducive to diffusion of macromolecular substrates (Fig. 2F). Confocal laser microscopy (CLSM) images provide visual confirmation of the spatial arrangement of FITC-labeled PmHS2 at the central core of the MOFs, indicating successful encapsulation and homogeneous distribution of enzymes within the MOFs (Fig. 2G-I).

All of the MOF-based microreactors prepared by varying reagent ratios, displayed accessible mesoporous porosity, as substantiated by $\rm N_2$ adsorption-desorption isotherms. Before the gas sorption measurements, lattice guest molecules, such as water, were meticulously removed $\it via$ solvent exchange followed by thermal activation at 120 °C for 12 h under a stream $\rm N_2$ (Fig. 2B). The pore-size distribution of microreactor 4N was calculated using nonlocal density functional theory (NLDFT) assuming a spherical pore geometry. The calculated pore width distribution revealed the presence of mesopores with maxima at $\sim\!\!4$ nm (Fig. 2C). Compared to the commonly synthesized microporous structure of zeolitic imidazolate framework material 90 (ZIF-90), the microreactor 4N possesses a mesoporous structure that facilitates the efficient diffusion of macromolecular polysaccharides into the microreactor pores.

The PmHS2-encapsulated microreactor was used as a biocatalyst for the synthesis of heparosan in a reaction system containing an acceptor/ donor molar ratio of GlcA-pNP: UDP-GlcNAc: UDP-GlcA = 1:10:10 in excellent 99 % conversion rate. Heparosan synthesized by microreactor 1N exhibited lower dispersity compared to those produced by free PmHS2 (Fig. 3A). Notably, the size of these polymers exhibited a linear correlation with the metal ion/ligand molar ratio of the catalyst in the synthetic reactions (Fig. 3B). With an increase in the organic ligand content of the immobilized material, the MOF structure became denser, featuring fewer defects and smaller pore sizes. Consequently, the heparosan polymers obtained catalytically displayed a lower molecular weight and narrower PDI. Considering both product molecular weight and yield, microreactor 4N emerged as the optimal catalyst for the synthesis of LMW-HS. Interestingly, when GlcA, GlcNAc-α1,4-GlcA-pNP, and GlcNTFA-α1,4-GlcA-pNP (Wu et al., 2015) were used as acceptors, the resulting heparosan polymers exhibited similar molecular weight distributions as shown in PAGE analysis (Fig. 3C), demonstrating that the molecular weights of products obtained from catalysts with fixed pore sizes are similar.

To synthesize 6-O-sulfated HS, the heparosan obtained from the microreactor 4N was treated with excess sulfur trioxide trimethylamine complex in formamide at 60 °C (Li et al., 2019). Gel permeation chromatography-multi-angle laser light scattering (GPC-MALLS) was used to determine the molecular weight of chemically 6-O-sulfated HS utilizing heparin and LMWHs (danaparoid sodium and enoxaparin sodium) as controls (Fig. 3D). Heparin exhibited an average molecular

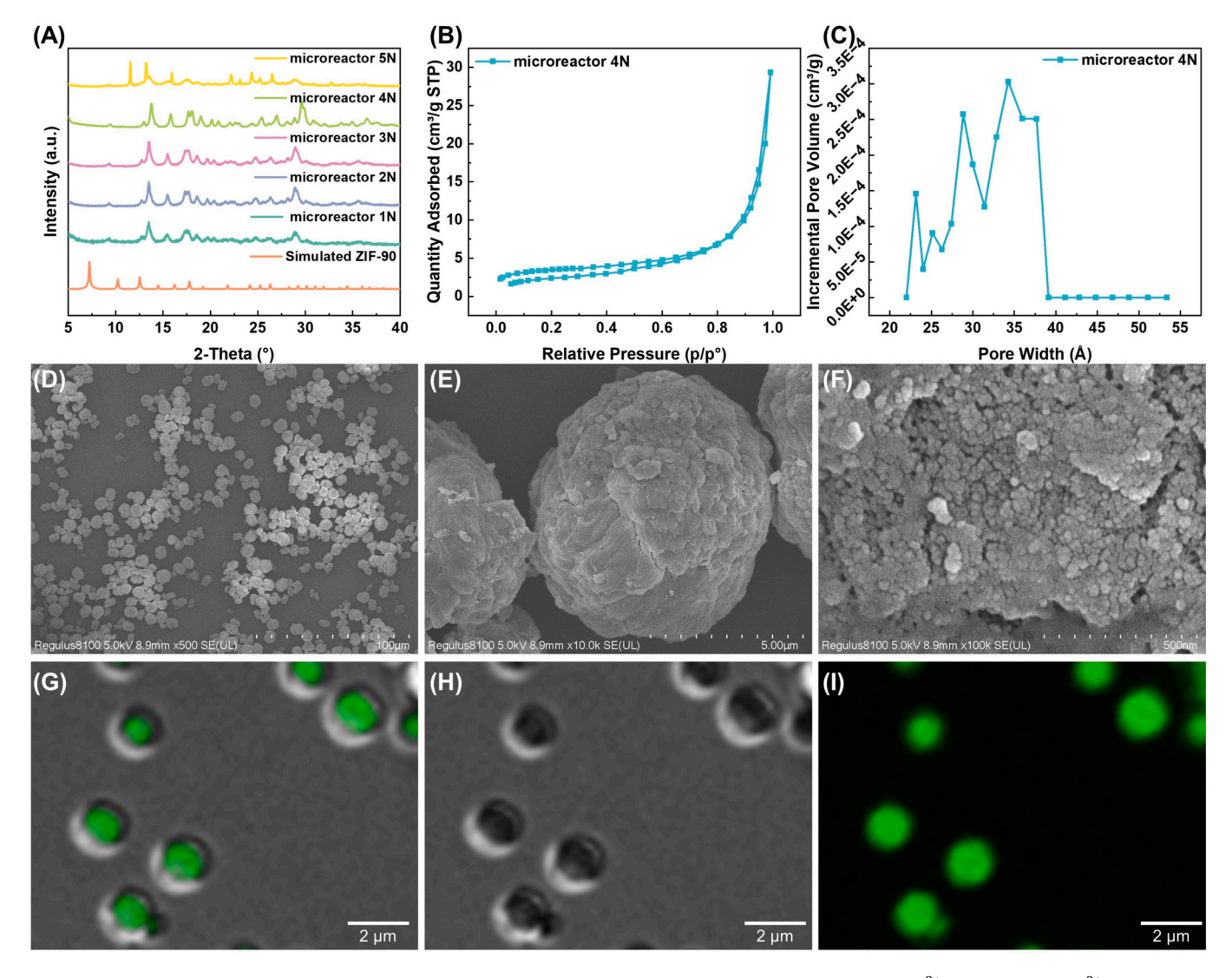


Fig. 2. (A) PXRD patterns of the synthesized microreactor using different ratios of metal ions and organic ligands. 1N: Zn^{2+} : ICA = 1:1, 2N: Zn^{2+} : ICA = 1:2, 3N: Zn^{2+} : ICA = 1:3, 4N: Zn^{2+} : ICA = 1:4, 5N: Zn^{2+} : ICA = 1:5. (B) Nitrogen adsorption and desorption isotherms at 77.3 K. (C) Pore size distributions of microreactor 4N calculated by NLDFT. (D—F) SEM image of microreactor 4N. CLSM images of microreactor 4N, (G) merged image, (G) bright-field, (I) excitation at 488 nm and monitoring the fluorescence of the FITC-labeled PmHS2 at 520 nm.

weight of 20,400 Da with a PDI of 1.064 (Fig. 3E). Danaparoid sodium and enoxaparin sodium gave Mw values of 9165 Da and 5056 Da, with PDI of 1.143 and 1.157, respectively (Fig. 3E-F). As expected, the molecular weights of 6-O-sulfated HS were precisely controlled at 6231 Da, featuring a remarkably narrow size distribution with a PDI of 1.032 (Fig. 3G). In summary, the synthesized HS polysaccharide based on NRPS exhibits low dispersity and controllable sugar chain length.

The synthesis of sugar chains of low dispersity can be attributed to the incorporation of MOF. First, unlike the free enzyme that facilitates continuous linear polymerization through the organized attachment of sugar donors to the non-reducing end of the growing polysaccharide chain (Fig. 4A), encapsulated enzymes impose space limitations on the glycosylation reaction. The pore size confined microreactor embeds the non-reducing end of the sugar chain, impeding further extension of the chain (Fig. 4B). Second, in the predicted glycosyltransferase-catalyzed process, the sugar-transfer reaction commences with UDP-sugar bond cleavage, leading to the formation of the UDP leaving group (Gómez et al., 2013; Mendoza et al., 2016). The accumulation of UDP results in a reverse glycosylation reaction, leading to a more polydisperse polysaccharide. In our catalytic system, the exposed metal sites of the MOF chelate the electronegative UDP, thereby inhibiting undesirable trans-

cleavage (i.e. reverse glycosylation). Additionally, using molecular docking analysis, the exposed metal sites on the MOFs and the negative oxygen ions on the pyrophosphate bond of UDP form a strong hydrogen bond at a distance of 1.7Å. The binding energy of UDP to MOF was -10.22 kcal/mol, significantly lower than that to the enzyme (-4.96 kcal/mol), providing computational support that MOF preferentially facilitates UDP removal from the intraparticle solution (Fig. 4C-D, Table 1).

Successful 6-*O*-sulfation was verified by 1 H NMR with characteristic chemical shifts of proton H6 of GlcNAc6S at \sim 4.10 and \sim 4.35 ppm (Fig. 5B) (Li et al., 2019; Zhang et al., 2017). The sulfated residues in heparin and enoxaparin were determined to be 52.1 % and 54.4 %, respectively. Consistent with expectation, the sulfated contents of chemically 6-*O*-sulfated HS was 27.7 % (Fig. 5B, Fig. S1-2).

To evaluate the anticoagulant activity of synthetic LMW 6-O-sulfated HS, activated partial thromboplastin time (APTT), prothrombin time (PT), and thrombin time (TT) assay were performed. Deionized water served as a negative control, while heparin and LMWH (danaparoid sodium and enoxaparin sodium) acted as positive controls. The 6-O-sulfated HS exhibited negligible anticoagulant activities (Fig. 5C, Fig. S3–5). As a clinically used anticoagulant, even though heparin has

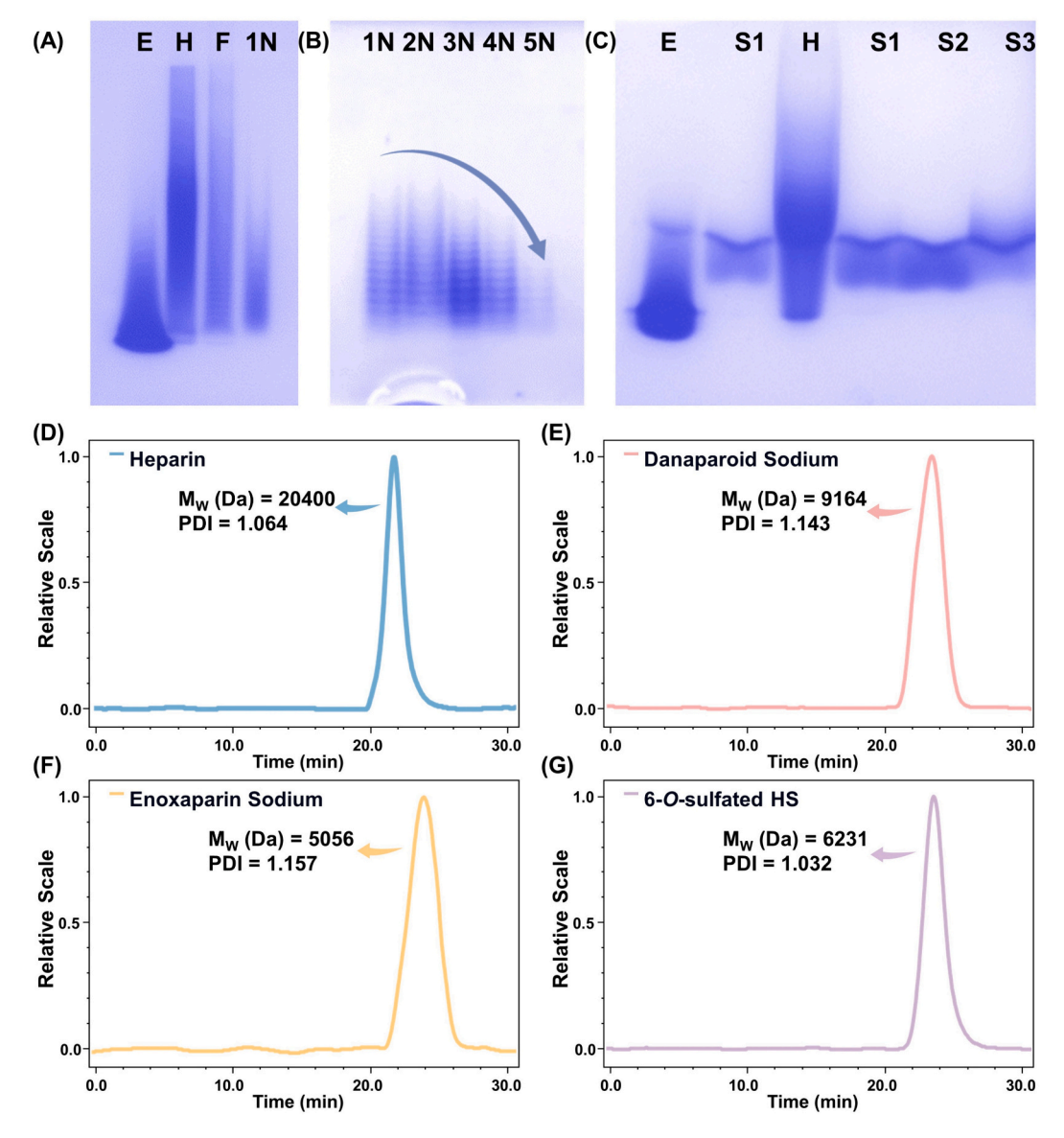


Fig. 3. (A) to (C): PAGE images of the heparosan polymers: (A) Comparison of heparosans synthesized with free and encapsulated enzymes, Lane E: enoxaparin sodium, Lane H: heparin, Lane F: heparosan prepared by free PmHS2, Lane1N: heparosan prepared by microreactor 1N; (B) Comparison of the distribution of heparosans synthesized with different encapsulated enzymes (microreactors), Lane1N: microreactor 1N, Lane 2N: microreactor 2N, Lane 3N: microreactor 3N, Lane 4N: microreactor 4N, Lane 5N: microreactor 5N; (C) Comparison of molecular weight of heparosans synthesized with microreactor 4N using varied sugar acceptors, Lane E: enoxaparin sodium, Lane H: heparin, Lane S1: GlcA, Lane S2: GlcNAc-α1,4-GlcA-pNP, Lane S3: GlcNTFA-α1,4-GlcA-pNP. (D) to (G): Molecular weight distribution analysis using GPC-MALLS: (D) heparin, (E) danaparoid sodium, (F) enoxaparin sodium, (G) 6-O-sulfated HS.

numerous biological and pharmacological activities, its medical applications has been limited due to concerns about hemorrhagic complications (Linhardt & Toida, 2004). Therefore, this synthesis of nonanticoagulant 6-O-sulfated HS could have potentials for the development of HS-based therapeutics (Ouyang et al., 2019). Fibroblast growth factors (FGFs), exhibit a high affinity for HS, play a crucial role in promoting epithelial repair and reducing myofibroblast differentiation and collagen production by fibroblasts (Sancar et al., 2022; Xie et al., 2020). In this study, the binding affinities between FGF1 and commercial LMWH or the synthetic 6-O-sulfated HS were evaluated by SPR (Fig. 5D-E). The kinetic parameters of the interactions between each polysaccharide and FGF1 are summarized in Table 2, with real-time sensorgrams depicted. Despite the synthetic 6-O-sulfated HS possessing only half the sulfation content of enoxaparin, the binding capacity of the synthetic 6-O-sulfated HS to FGF1 was comparable to commercial LMWH. In addition, it is well known that the interactions of HS with proteins are largely related to the degree of sulfation, thereby suggesting that an elevated degree of sulfation may lead to an augmentation of undesired side effects (Sargison et al., 2022). This demonstrates that our synthesized 6-O-sulfated HS could provide basic biological activity with reduced anticoagulant and other side effects.

3. Conclusion

In this study, a nanopore-regulated polymerization strategy (NPRS) was developed to catalyze the size controllable polymerization of glycans using MOF-encapsulated glycosyltransferase. This strategy is efficient, reusable and does not require stepwise isolation and purification processes. Specifically, we prepared immobilized glycosyltransferase composites based on a mesoporous MOF through a perturbation-assisted nanofusion strategy. The generation of mesopores facilitated the efficient transfer of macromolecular substrates between the reaction solution and the enzyme, overcoming the limitation of traditional microporous MOFs in polysaccharide synthesis. The spatial confinement

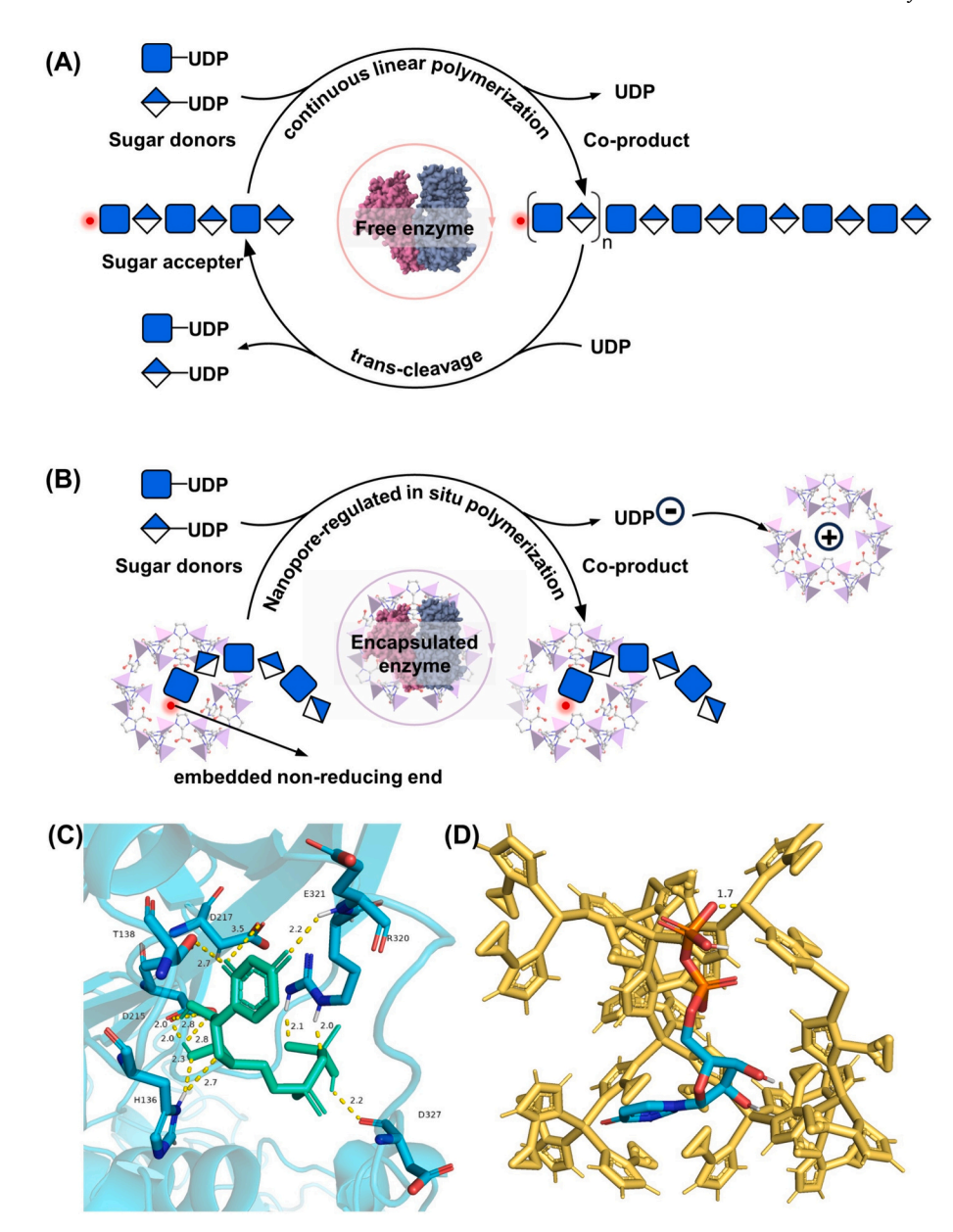


Fig. 4. Differences in the glycosylation reactions catalyzed by free enzymes (A) and encapsulated enzymes (B); Molecular docking of UDP and PmHS2 (C), and UDP and Zn^{2+} -ICA MOF (D).

Table 1Docking Calculations between UDP and PmHS2 or MOF.

Acceptor	Binding energy (kcal/mol) ^a	Inhibition constant	
PmHS2	-4.96	232.23 μM	
MOF	-10.22	32.35 nM	

^a Binding energy between UDP and PmHS2 or MOF under optimal conformational conditions.

of the shield/armor of MOFs played a crucial role in constraining the glycosylation reaction, leading to lower molecular weight polysaccharides. Moreover, competitive adsorption of UDP co-product by MOFs contributed to significantly inhibiting undesired trans-cleavage and enhancing the homogeneity of the catalytic products. Homogeneous low molecular weight 6-O-sulfated HS (MW \sim 6 kDa) of low dispersity with low PDI (1.032), was successfully prepared using this one-pot synthetic procedure. The synthesized 6-O-sulfated HS

demonstrated low anticoagulant activity while maintaining its FGF1 binding affinity comparable to enoxaparin. We believe the current study provides an example that *in situ* polymerization can be regulated by the nanopororous microenvironment of the metal-organic capsule. It is anticipated that this work will expedite the exploration of more MOFs with specific pore sizes to prepare glycosaminoglycans with controlled molecular sizes. An in-depth understanding of the intricate interaction between sugar chains, glycosyltransferases and MOFs will promote the rapid and efficient synthesis of homogeneous HS-related drugs of low dispersity.

4. Experimental section

4.1. Materials

High Affinity Ni-Charged Resin FF was purchased from GenScript (Nanjing, China). Tryptone, Yeast extract, Amicon® Ultra-15 Centrifugal Filter Unit (30 kDa), Imidazole(C₃H₄N₂), Zinc nitrate hexahydrate

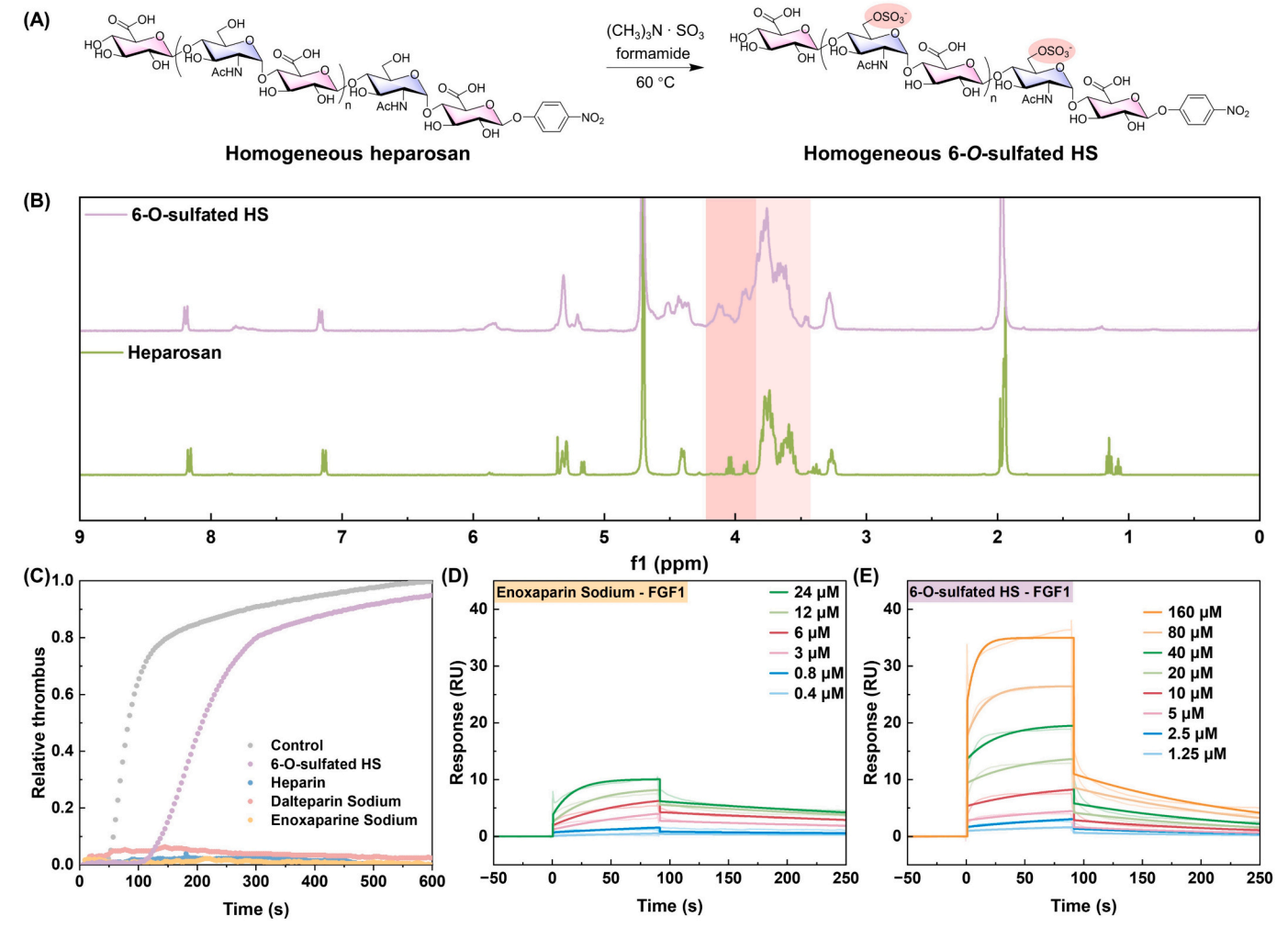


Fig. 5. (A) Schematic diagram of the 6-O-sulfation of HS. (B) ¹H NMR spectra of the synthesized heparosan and 6-O-sulfated product. (C) Anticoagulant activityanalysis heparin, LMWHs and synthetic 6-O-sulfated HS on the prolongation of APTT at a concentration of 500 μg/mL. (D) to (E): SPR sensorgrams of FGF1 binding to enoxaparin sodium (D) and 6-O-sulfated HS (E).

Table 2Kinetic parameters s for the interactions of LMWH and 6-O-sulfated HS with FGF1.

Sample	$k_a (1/Ms)^a$	$k_d (1/s)^b$	K_D (M) ^c
6-O-sulfated HS	837.1	0.0066	7.84E-06
Enoxaparin sodium	2175	0.0025	1.13E-06

^a k_a: association rate constant.

(Zn(NO₃)₂·6H₂O), 2-Imidazolecarboxaldehyde (ICA, C₄H₄N₂O), Uridine 5'-diphosphoglucuronic Acid Trisodium (UDP-GlcA), Uridine 5'-diphospho-*N*-acetylglucosamine sodium salt (UDP-GlcNAc), *p*-Nitrophenyl- β -D-glucuronide (GlcA-*p*NP) were purchased from Sigma Aldrich (Shanghai, China). Bradford Protein Assay Kit was purchased from Beyotime (Shanghai, China).

4.2. Expression and purification of PmHS2

The procedure of expression and the purification of the recombinant proteins PmHS2 was described previously in our published work (Qiao et al., 2022).

4.3. Synthesis of PmHS2-encapsulated microreactor

The 2-Imidazolecarboxaldehyde solution (0.4/0.8/1.2/1.6/2 mL, 240 mM) and PmHS2 aqueous solution (2 mg PmHS2 in 2.4/2/1.6/1.2/0.8 mL $\rm H_2O)$ were mixed in a 5 mL PE tube, followed by the addition of zinc nitrate solution (0.4 mL, 240 mM). The reaction solution was placed on long axis mixer (RT, 25 rpm, 12 h). Finally, the supernatant after centrifugation (8000 rpm, 3 min) of the reaction solution was taken to test the immobilization efficiency, and the precipitate was washed, centrifuged with ultrapure water for three times to completely remove the free enzyme.

4.4. Characterization of synthesized metal-organic capsule

Powder X-ray diffraction (PXRD) patterns of samples were recorded on a Rigaku SmartLab at 9 KeV in Bragg-Brentano geometry. Sample morphology was analyzed utilizing HITACHI SU8100 high resolution field emission scanning electron microscope (SEM). $\rm N_2$ adsorption-desorption isotherms were collected with a micromeritics ASAP 2460 at 77 K. The sample were pre-treated at 120 $^{\circ}\mathrm{C}$ for 12 h before measurements. The confocal laser microscopy (CLSM) images were demonstrated by Nikon AX with the excitation at 488 nm.

 $^{^{\}text{b}}$ k_{d} : dissociation rate constant.

^c K_D: apparent equilibrium dissociation constant.

4.5. Synthesis of heparosan polysaccharide

The heparosan polysaccharide was synthesized by incubating a mixture containing 100 mM Tris-HCl, pH 7.5, 10 mM MnCl $_2$, 10 mM UDP-GlcNAc,10 mM UDP-GlcA, 1 mM GlcA-pNP, and PmHS2 or PmHS2-encapsulated microreactor with the total volume of 200 μ L at 37 °C for 12 h. In the large-scale synthesis of homogeneous low molecular weight heparosan of low dispersity, 3 mg GlcA-pNP (0.01 mmol), 65 mg UDP-GlcNAc (0.1 mmol), and 62 mg UDP-GlcNAc (0.1 mmol) were reacted in 10 mL of aqueous solution with microreactor 4N (0.5 mg/mL). After centrifugation, the supernatant was used to determine the conversion rate by HPLC analysis for residual glycosyl accepters and then purified with Amicon® Ultra-15 Centrifugal Filter Unit (3 kDa) by centrifugation (6000 rpm). The purified heparosan polysaccharide was lyophilized to give 37 mg white solid with yield of 90 % and analyzed by polyacrylamide gel electrophoresis (PAGE), gel permeation chromatography (GPC).

4.6. Preparation of the 6-O-sulfated LMW-HS by chemical method

The heparosan polysaccharide was dissolved in formamide and a sulfur trioxide trimethylamine complex ($\sim \! 10$ equiv. per free hydroxyl group was added, based on the number of oligosaccharide units in the side chain). The reaction was stirred at 60 °C overnight. All the products were transferred into ethanol at room temperature before the addition of 16 % aqueous NaCl. After neutralizing by adding saturated sodium bicarbonate solution, the reaction was dialyzed (MWCO: 1 kDa) against distilled water for 2 days, and the dialysate was lyophilized to give a white powder, which was dissolved in 16 % aqueous NaCl. The addition of four volumes of ethanol and centrifugation at 12,000 rpm for 10 min yielded the precipitated product, which was then dissolved in water and dialyzed (MWCO = 1 kDa) against distilled water for 2 days. The dialysate was lyophilized to give a white solid.

4.7. NMR spectroscopy analysis

For NMR analysis, the samples were freeze-dried with 500 μL of D_2O (99.9 %) three times before final dissolution in 500 μL of D_2O (99.9 %). The NMR experiments were conducted on an Agilent DD2 500 MHz Nuclear Magnetic Resonance Spectrometer (Agilent, USA) at room temperature. The sulfate contents were calculated by the integral ratio of the samples in two intervals of 3.40–3.90 ppm and 3.90–4.35 ppm.

$$sulfate\ contents = \int_{3.9-4.35\ ppm} \bigg/ \bigg(\int_{3.4-3.9\ ppm} + \int_{3.9-4.35\ ppm} \bigg)$$

4.8. Molecular weight determination of heparinoids by HPGPC-MALLS

Using the Agilent 1260 High Performance Liquid Chromatography system (Agilent, Santa Clara, CA, USA), a Dawn Heleos-II multi-angle laser scattering instrument and a moving index detector (Wyatt Technology, Santa Barbara, CA, USA) to determine the molecular weight of the compound. Gel chromatography was performed with Shodex OHpak SB-803 HQ and SB-802.5 HQ columns at a flow rate of 0.6 mL/min and a moving phase of 0.1 mol/L NaNO3. The sample concentration was 5 mg/mL and the analysis was performed at 35 °C for 45 min. The dn/dc value of heparinoids in 0.1 M NaNO3 solution was calculated as 0.1209 mL/g at 658 nm. Wyatt ASTRA v 6.1.1 software was used to analyze the data.

4.9. In vitro anticoagulant activity

APTT, TT, and PT assays were performed according to the established methods (Ma et al., 2019). 6-O-sulfated heparan sulfate (HS) was dissolved in dd $\rm H_2O$ at concentrations of 0.5, 1, 2, 3, 4, 5, 10, 15, 20, and 30 mg/mL. For APTT assay, 45 μL of sheep plasma and 5 μL of polysaccharide solution was mixed with 50 μL of pre-warmed APTT reagent

and cultured at 37 °C for 3 min. Then, 50 µL of pre-warmed CaCl₂ (0.025 mol/L) was added and clotting time was measured in a C2000-4 Semiautomatic coagulator (Beijing PULisen Instrument CO., LTD., Beijing, China). To further ensure the accuracy of anticoagulation, the changes in the absorbance while measuring the APTT at a concentration of 500 µg/mL, corresponding to the fibrin formation, was monitored with microplate reader at a wavelength of 500 nm (Biotek Synergy H1). Deionized water was used as a negative control, while heparin, dalteparin sodium, and enoxaparin sodium were used as positive controls at the concentration of 500 $\mu g/mL$. For PT assay, 45 μL of sheep plasma was mixed with 5 μL of polysaccharide solution and cultured at 37 $^{\circ}C$ for 3 min. Then, 50 μL of pre-warmed PT assay reagent was added and clotting time was measured. For TT assay, the same mixture of sheep plasma and samples, followed by the addition of 45 μL of TT reagent, was determined. Enoxaparin sodium was used as the positive control, and dd H₂O was used as the negative control.

4.10. SPR analysis of the protein interactions with HS

The SPR experiment was carried out using the Biacore T200 SPR spectrometer (Cytiva, Uppsala, Sweden) according to a reported method (Yanucil et al., 2022). To prepare FGF1 chip using amine coupling, CM5 chip was activated by injecting with a mix solution of 0.4 M EDC with 0.1 M NHS for 900 s at a flow rate of 10 µL/min. Immediately after activation, 20 µg/mL of FGF1 in sodium acetate buffer (10 mM, pH 5.0) was injected to flow channel 2 for 900 s, followed by the injection of ethanolamine (1 M, pH 8.5) for 450 s to block the remaining activated sites. The final FGF1 immobilized amount was 7924 RU. The same procedures for activation and blocking were repeated on flow cell 1 which was used as negative control for the interaction analysis. Varying concentrations of LMWH and LMW-HS in PBS-P running buffer (0.02 M phosphate buffer with 2.7 mM KCl, 0.137 M NaCl and 0.05 % Surfactant P20, pH 7.4) were injected over the FGF1 chip for 90 s at 30 μL/min, followed by a dissociation phase for 120 s. Finally, the regeneration was carried out with 5 mM NaOH for 30 s. The response was monitored as a function of time (sensorgram) at 25 °C and subtracted from the response of the reference surface (control). Kinetic parameters were obtained thorough global fitting entire association and dissociation phases by employing a 1:1 binding model from the BlA evaluation software 4.1.

CRediT authorship contribution statement

Meng Qiao: Writing – original draft, Methodology, Data curation. Zhe Wang: Software, Methodology, Data curation. Junjie Zhang: Investigation. Yanqi Li: Visualization. Liang-An Chen: Investigation. Jonathan S. Dordick: Writing – review & editing, Funding acquisition. Robert J. Linhardt: Writing – review & editing, Funding acquisition. Chao Cai: Supervision, Conceptualization. He Huang: Supervision, Project administration. Xing Zhang: Writing – review & editing, Funding acquisition, Conceptualization.

Declaration of competing interest

We declare that we have no known competing financial interests or personal relationships that could have appeared to influence the work reported in this paper.

Data availability

Data will be made available on request.

Acknowledgement

This research was funded by National Key Research and Development Project of China 2021YFC2100100 (X. Z.), Taishan Scholar Young Project TSQN202306099 (C. C.), National Science Foundation GlycoMIP

DMR 1933525 (R.J. L, F. Z., and J.S. D), and Postgraduate Research & Practice Innovation Program of Jiangsu Province KYCX24_1861 (M. Q.).

Appendix A. Supplementary data

Supplementary data to this article can be found online at https://doi.org/10.1016/j.carbpol.2024.122297.

References

- An, H., Song, J., Wang, T., Xiao, N., Zhang, Z., Cheng, P., ... Chen, Y. (2020). Metalorganic framework disintegrants: Enzyme preparation platforms with boosted activity. Angewandte Chemie International Edition, 59, 16764–16769.
- Arbulu, R. C., Jiang, Y. B., Peterson, E. J., & Qin, Y. (2018). Metal-Organic framework (MOF) nanorods, nanotubes, and nanowires. Angewandte Chemie International Edition. 57, 5813–5817.
- Arnold, K., Xu, Y., Liao, Y.-E., Cooley, B. C., Pawlinski, R., & Liu, J. (2020). Synthetic anticoagulant heparan sulfate attenuates liver ischemia reperfusion injury. Scientific Reports. 10. 17187.
- Chen, G., Kou, X., Huang, S., Tong, L., Shen, Y., Zhu, W., Zhu, F., & Ouyang, G. (2020). Modulating the biofunctionality of metal-organic-framework-encapsulated enzymes through controllable embedding patterns. *Angewandte Chemie International Edition*, 59, 2867–2874.
- Chen, T. T., Yi, J. T., Zhao, Y. Y., & Chu, X. (2018). Biomineralized metal-organic framework nanoparticles enable intracellular delivery and endo-lysosomal release of native active proteins. *Journal of the American Chemical Society*, 140, 9912–9920.
- Clausen, T. M., Sandoval, D. R., Spliid, C. B., Pihl, J., Perrett, H. R., Painter, C. D., ... Esko, J. D. (2020). SARS-CoV-2 infection depends on cellular heparan sulfate and ACE2. *Cell*, *183*, Article 1043-1057.e1015.
- Gómez, H., Lluch, J. M., & Masgrau, L. (2013). Substrate-assisted and nucleophilically assisted catalysis in bovine a1,3-galactosyltransferase. Mechanistic implications for retaining glycosyltransferases. *Journal of the American Chemical Society*, 135, 7053–7063.
- Huang, S., Kou, X., Shen, J., Chen, G., & Ouyang, G. (2020a). "Armor-Plating" enzymes with metal-organic frameworks (MOFs). Angewandte Chemie, International Edition, 59, 8786–8798.
- Huang, S., Kou, X., Shen, J., Chen, G., & Ouyang, G. (2020b). "Armor-Plating" enzymes with metal–organic frameworks (MOFs). Angewandte Chemie International Edition, 59, 8786–8798.
- Li, J., Li, J., Sun, T., Cai, C., Shao, M., & Yu, G. (2019). Concise chemoenzymatic synthesis of heparan sulfate analogues as potent BACE-1 inhibitors. *Carbohydrate Polymers*, 217, 232–239.
- Li, S., Wang, S., Fu, X., Liu, X.-w., Wang, P. G., & Fang, J. (2017). Sequential one-pot multienzyme synthesis of hyaluronan and its derivative. *Carbohydrate Polymers*, 178, 221–227.
- Linhardt, R. J., & Toida, T. (2004). Role of glycosaminoglycans in cellular communication. Accounts of Chemical Research, 37, 431–438.
- Liu, C., Lin, L., Sun, Q., Wang, J., Huang, R., Chen, W., ... Yu, C. (2020). Site-specific growth of MOF-on-MOF heterostructures with controllable nano-architectures: Beyond the combination of MOF analogues. *Chemical Science*, 11, 3680–3686.
- Liu, H., Zhang, Z., & Linhardt, R. J. (2009). Lessons learned from the contamination of heparin. Natural Product Reports, 26, 313–321.
- Ma, L., Huang, J., Zhu, X., Zhu, B., Wang, L., Zhao, W., Qiu, L., Song, B., Zhao, C., & Yan, F. (2019). In vitro and in vivo anticoagulant activity of heparin-like biomacromolecules and the mechanism analysis for heparin-mimicking activity. *International Journal of Biological Macromolecules*, 122, 784–792.
- McGowan, K. E., Makari, J., Diamantouros, A., Bucci, C., Rempel, P., Selby, R., & Geerts, W. (2016). Reducing the hospital burden of heparin-induced thrombocytopenia: Impact of an avoid-heparin program. *Blood*, 127, 1954–1959.
- Mende, M., Bednarek, C., Wawryszyn, M., Sauter, P., Biskup, M. B., Schepers, U., & Bräse, S. (2016). Chemical synthesis of glycosaminoglycans. *Chemical Reviews*, 116, 8193–8255

- Mendoza, F., Gómez, H., Lluch, J. M., & Masgrau, L. (2016). α1,4-N-Acetylhexosaminyltransferase EXTL2: The missing link for understanding glycosidic bond biosynthesis with retention of configuration. ACS Catalysis, 6, 2577–2589.
- Ouyang, Y., Yu, Y., Zhang, F., Chen, J., Han, X., Xia, K., ... Linhardt, R. J. (2019). Non-anticoagulant low molecular weight heparins for pharmaceutical applications. *Journal of Medicinal Chemistry*, 62, 1067–1073.
- Pawar, N. J., Wang, L., Higo, T., Bhattacharya, C., Kancharla, P. K., Zhang, F., ... Hsieh-Wilson, L. C. (2019). Expedient synthesis of core disaccharide building blocks from natural polysaccharides for heparan sulfate oligosaccharide assembly. *Angewandte Chemie International Edition*, 58, 18577–18583.
- Qiao, M., Ji, Y., Linhardt, R. J., Zhang, X., & Huang, H. (2022). Fabricating bimetal organic material capsules with a commodious microenvironment and synergistic effect for glycosyltransferase. ACS Applied Materials & Interfaces, 14, 26034–26043.
- Sancar, G., Liu, S., Gasser, E., Alvarez, J. G., Moutos, C., Kim, K., ... Evans, R. M. (2022). FGF1 and insulin control lipolysis by convergent pathways. *Cell Metabolism*, 34, 171–183.e176.
- Sargison, L., Smith, R. A. A., Carnachan, S. M., Daines, A. M., Brackovic, A., Kidgell, J. T., ... Hinkley, S. F. R. (2022). Variability in the composition of porcine mucosal heparan sulfates. *Carbohydrate Polymers*, 282, Article 119081.
- Spadarella, G., Di Minno, A., Donati, M. B., Mormile, M., Ventre, I., & Di Minno, G. (2020). From unfractionated heparin to pentasaccharide: Paradigm of rigorous science growing in the understanding of the in vivo thrombin generation. *Blood Reviews*, 39, Article 100613.
- Stancanelli, E., Liu, W., Su, G., Padagala, V., & Liu, J. (2024). Developing a solid-phase method for the enzymatic synthesis of heparan sulfate and chondroitin sulfate backbones. *Glycobiology*, 34, Article cwad093.
- Wang, Y., Li, S., Xu, X., Tan, Y., Liu, X.-w., & Fang, J. (2020). Chemoenzymatic synthesis of homogeneous chondroitin polymers and its derivatives. *Carbohydrate Polymers*, 232, Article 115822.
- Wang, Z., Arnold, K., Dhurandahare, V. M., Xu, Y., Pagadala, V., Labra, E., ... Liu, J. (2022). Analysis of 3-O-sulfated heparan sulfate using isotopically labeled oligosaccharide calibrants. *Analytical Chemistry*, 94, 2950–2957.
- Wang, Z., Arnold, K., Dhurandhare, V. M., Xu, Y., & Liu, J. (2021). Investigation of the biological functions of heparan sulfate using a chemoenzymatic synthetic approach. RSC Chemical Biology, 2, 702–712.
- Wu, B., Wei, N., Thon, V., Wei, M., Yu, Z., Xu, Y., ... Li, T. (2015). Facile chemoenzymatic synthesis of biotinylated heparosan hexasaccharide. *Organic & Biomolecular Chemistry*, 13, 5098–5101.
- Xie, Y., Su, N., Yang, J., Tan, Q., Huang, S., Jin, M., ... Chen, L. (2020). FGF/FGFR signaling in health and disease. Signal Transduction and Targeted Therapy, 5, 181.
- Xu, Y., Cai, C., Chandarajoti, K., Hsieh, P.-H., Li, L., Pham, T. Q., ... Liu, J. (2014). Homogeneous low-molecular-weight heparins with reversible anticoagulant activity. *Nature Chemical Biology*, 10, 248–250.
- Xu, Y., Masuko, S., Takieddin, M., Xu, H., Liu, R., Jing, J., ... Liu, J. (2011). Chemoenzymatic synthesis of homogeneous ultralow molecular weight heparins. *Science*, 334, 498–501.
- Yanucil, C., Kentrup, D., Campos, I., Czaya, B., Heitman, K., Westbrook, D., ... Faul, C. (2022). Soluble α-klotho and heparin modulate the pathologic cardiac actions of fibroblast growth factor 23 in chronic kidney disease. *Kidney International*, 102, 261–279
- Yue, Y., Fulvio, P. F., & Dai, S. (2015). Hierarchical metal-organic framework hybrids: Perturbation-assisted nanofusion synthesis. Accounts of Chemical Research, 48, 3044–3052
- Yue, Y., Qiao, Z.-A., Fulvio, P. F., Binder, A. J., Tian, C., Chen, J., ... Dai, S. (2013). Template-free synthesis of hierarchical porous metal-organic frameworks. *Journal of the American Chemical Society*, 135, 9572–9575.
- Zhang, P., Lu, H., Peixoto, R. T., Pines, M. K., Ge, Y., Oku, S., ... Craig, A. M. (2018). Heparan sulfate organizes neuronal synapses through neurexin partnerships. *Cell*, 174, Article 1450-1464.e1423.
- Zhang, X., Lin, L., Huang, H., & Linhardt, R. J. (2020). Chemoenzymatic synthesis of glycosaminoglycans. Accounts of Chemical Research, 53, 335–346.
- Zhang, X., Pagadala, V., Jester, H. M., Lim, A. M., Pham, T. Q., Goulas, A. M. P., ... Linhardt, R. J. (2017). Chemoenzymatic synthesis of heparan sulfate and heparin oligosaccharides and NMR analysis: Paving the way to a diverse library for glycobiologists. *Chemical Science*, 8, 7932–7940.